# Numerical simulation and design of casting system for stainless steel exhaust manifold

*Pei-Hsing* Huang[1,*], *Jenn-Kun* Kuo[2], *Te-Hua* Fang[3], and *Wei-ren* Wu[1]

[1]Department of Mechanical Engineering, National Pingtung University of Science and Technology, Pingtung 912, Taiwan

[2]Department of Greenergy, National University of Tainan, Tainan 70005, Taiwan

[3]Department of Mechanical Engineering, National Kaohsiung University of Applied Sciences, Kaohsiung 807,Taiwan

**Abstract.** During operation, exhaust manifolds must bear the corrosion of high temperatures and repeated stress, which can easily lead to cavitation, corrosion, and creeping damage in the casting structure and affect product safety. To improve the structure of exhaust manifolds and increase their service life, we employed AnyCasting mold flow analysis to SUS304 stainless steel exhaust manifolds. We examined the influence of casting system design and process parameters such as ceramic shell temperature, casting temperature, and pouring speed on the filling and solidification processes of the liquid metal. Finally, we used the Niyama criterion to predict the probability and distribution of shrinkage porosity defects in the exhaust manifold and made improvements to enhance the quality of exhaust manifold castings. Keywords: exhaust manifold, mold flow analysis, casting system.

## 1 Introduction

The casting industry has thousands of years of history, but developments in casting technology are still being made. Casting products must undergo strict quality inspections to meet relevant specifications. Improving various casting defects is the goal of the casting industry, and to enhance casting quality and yield while reducing labor costs, many researchers have developed molten metal flow analysis methods for casting defect prediction using computer-aided engineering (CAE) [1-10]. At present, the majority of casting manufacturers in Taiwan use trial and error to derive optimal casting schemes. During this process, manufacturers will produce castings with defects, which they then repair using welding, as shown in Fig. 1. Zhao et al. [11] used ProCAST to predict where shrinkage defects will appear in solidifying steel plates and compared the results with those of actual castings. Huang et al. [12] established that directly using open risers or blind risers cannot effectively prevent shrinkage cavity and porosity defects in stainless steel impeller castings, but coordinating the risers with cold iron can. Ma and Chuan [13] examined the

* Corresponding author: phhuang1970@gmail.com

differences in the internal mass of products before and after optimization and found that structural optimization can significantly enhance the performance of rear cover housing. Using the finite element method, Yang and Chi [14] simulated the temperature field of the casting solidification process and analyzed shrinkage cavity and porosity defects. Li and Peng [15] employed CAE software to simulate the solidification processes of a casting scheme and its improved scheme; the results indicated that the improved scheme simplified the moulding process and the riser elimination process, enabled effective feeding in the casting, and greatly reduced shrinkage defects. Sun et al. [16] developed a die casting process for automotive aluminium alloys, and the results demonstrated that optimizing the process parameters significantly reduced the shrinkage cavities and defects in the castings. Li et al. [17] analyzed the influence of riser designs on the feeding effects of gray cast iron pieces. The simulation results indicated that changing the height and diameter of riser necks can greatly improve riser feeding effects and reduce shrinkage defects in the casting products. This study used mold flow analysis to design a casting system for an exhaust manifold and adjust the process parameters so as to effectively enhance the quality and yield of exhaust manifold castings.

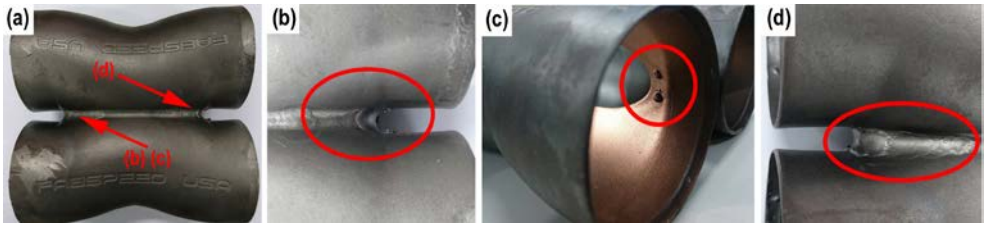


**Fig. 1.** Welded repairs on exhaust manifold; (a) locations of repairs on exhaust manifold; (b)-(d) welding and penetration marks of repaired defects circled in red.

## 2 Experimental and numerical methods

### 2.1 Process parameter settings of investment casting

We chose SUS304 stainless steel for this study, which is resistant to corrosion and high temperatures and has good mechanical properties. As a result, it is a suitable material for exhaust manifolds. We imported the physical properties of the SUS304 stainless steel into the metal mold flow analysis, which include density ( $\rho$ ): 7,930 kg/m3, thermal conductivity (K): 14.39 W/m·K, specific heat (S): 494 J/kg·K, latent heat (L): 290 kJ/kg, liquidus temperature ($T_l$): 1,454 °C, and solidus temperature ($T_s$): 1,399 °C, as shown in Table 1. We designed the process parameters of the initial scheme and the improved scheme based on the material characteristics. These properties and parameters include the liquidus and solidus temperatures, casting material ingredients, ceramic shell temperature $T_{ceramic}$ (°C), casting temperature $T_{casting}$ (°C), pouring speed $V_{pouring}$ (cm/s), and ceramic shell thickness $\delta$ (mm), as shown in Table 2.

**Table 1.** Thermophysical properties of SUS304 stainless steel [9].

| $\rho$ ( kg/m3) | K(W/m·K) | S(J/kg·K) | L(kJ/kg) | $T_l$ (°C) | $T_s$ (°C) |
|---|---|---|---|---|---|
| 7930 | 14.39 | 494 | 290 | 1454 | 1399 |

**Table 2.** Process parameters of casting schemes.

| | Initial scheme | Improved scheme |
|---|---|---|
| Casting material | SUS 304 | |
| Shell mold material | Zircon sand | |
| Mesh number | 3,000,000 | |
| $T_{ceramic}$ (°C) | 1050 | 1050 |
| $T_{casting}$ (°C) | 1600 | 1600 |
| $\delta(mm)$ | 6.0 | |
| $V_{pouring}$ (cm/s) | 7 | 9 |

## 2.2 Molten metal flow analysis and method

We performed numerical simulation and analysis for exhaust manifolds using the AnyCasting software package. The simulation process was divided into three major parts: pre-processing (physical model selection, meshing, and parameter setting), computation processing (flow field calculation, temperature field calculation, stress field calculation, and defect prediction analysis), and post-processing (result analysis). Furthermore, the continuity equation, the Navier-Stokes equations, energy equation, and volume function equation can be used to calculate the filling and solidification processes of the liquid metal and the changes in temperature, speed, and pressure, as shown in Eqs. (1)-(6) [1,8-10].

(1) Continuity equation:

$$\frac{\partial \rho}{\partial t}+\frac{\partial(\rho u)}{\partial x}+\frac{\partial(\rho v)}{\partial y}+\frac{\partial(\rho w)}{\partial z}=0 \tag{1}$$

(2) Navier-Stokes equations:

$$\rho\left(\frac{\partial u}{\partial t}+u\frac{\partial u}{\partial x}+v\frac{\partial u}{\partial y}+w\frac{\partial u}{\partial z}\right)=-\frac{\partial p}{\partial x}+\rho g_x+\mu\left(\frac{\partial^2 u}{\partial x^2}+\frac{\partial^2 u}{\partial y^2}+\frac{\partial^2 u}{\partial z^2}\right) \tag{2}$$

$$\rho\left(\frac{\partial v}{\partial t}+u\frac{\partial v}{\partial x}+v\frac{\partial v}{\partial y}+w\frac{\partial v}{\partial z}\right)=-\frac{\partial p}{\partial y}+\rho g_y+\mu\left(\frac{\partial^2 v}{\partial x^2}+\frac{\partial^2 v}{\partial y^2}+\frac{\partial^2 v}{\partial z^2}\right) \tag{3}$$

$$\rho\left(\frac{\partial w}{\partial t}+u\frac{\partial w}{\partial x}+v\frac{\partial w}{\partial y}+w\frac{\partial w}{\partial z}\right)=-\frac{\partial p}{\partial z}+\rho g_z+\mu\left(\frac{\partial^2 w}{\partial x^2}+\frac{\partial^2 w}{\partial y^2}+\frac{\partial^2 w}{\partial z^2}\right) \tag{4}$$

(3) Energy conservation equation:

$$\rho\frac{\partial H}{\partial t}+\rho H\nabla\cdot\vec{u}-\nabla\cdot(k\nabla T)-q=0 \tag{5}$$

(4) Volume function equation:

$$\frac{\partial F_V}{\partial t}+u_1\frac{\partial F_V}{\partial x}+u_2\frac{\partial F_V}{\partial y}+u_3\frac{\partial F_V}{\partial z}=0 \tag{6}$$

In this study, defect prediction was performed using the Niyama criterion [9,18], which predicts microscopic defects based on crystal formation within the castings.

$$G/\sqrt{R}<C_{Niyama} \tag{7}$$

In the Niyama criterion, a $G/\sqrt{R}$ value less than the threshold value means a greater probability of shrinkage porosity, whereas a $G/\sqrt{R}$ greater than the threshold value means a smaller probability of shrinkage porosity [18].

In Eqs. (1)-(7), $u$, $v$, and $w$ denote the speed vectors along the X, Y, and Z axes; $\rho$ represents density; $\mu$ is the dynamic viscosity of the liquid metal; $g_x$, $g_y$, and $g_z$ are the gravity acceleration vectors; $t$ denotes time; $q$ represents volume heat flux; $H$ is enthalpy; $G$ denotes the temperature gradient; $R$ represents to cooling rate, and $C_{Niyama}$ is the cooling rate.

## 3 Results and discussions

### 3.1 Mold flow analysis of initial scheme for exhaust manifold

The filling and solidification processes of the liquid metal are crucial to casting quality. We therefore incorporated AnyCasting numerical simulation and analysis to examine the cavity filling process, the directions of solidification and cooling, turbulent flows, and poured short, as shown in Fig. 2. As shown in Fig. 2 (a), the liquid metal flows vertically through the gate and fills the horizontal runner. It then enters the exhaust manifold via the ingate and encounters a surface, which creates impact and causes splashes and turbulent flows. Thus, the liquid metal cannot flow steadily into the exhaust manifold. The portions circles in red in Fig. 2(b) show that the surfaces of the exhaust manifold have already solidified, while the pipe junctions and runners have not. This means that the walls of the pipe junctions are thicker and have greater geometric changes. Furthermore, the solidification process of the pipe junction walls creates isolated residual melts on both the left and right sides. Figure 3 displays the probabilities and distributions of defects in the initial scheme. A darker red indicates a higher probability of shrinkage porosity defects, whereas a darker blue means a lower probability of shrinkage porosity defects. Figures 3(a) and 3(c) show larger areas with high probability of shrinkage porosity defects on top of the exhaust manifold near the ingates and at the bottom. Furthermore, the parts circled in red in Fig. 3(b) show a lot of gray areas at the pipe junctions, which mean poured short defects.

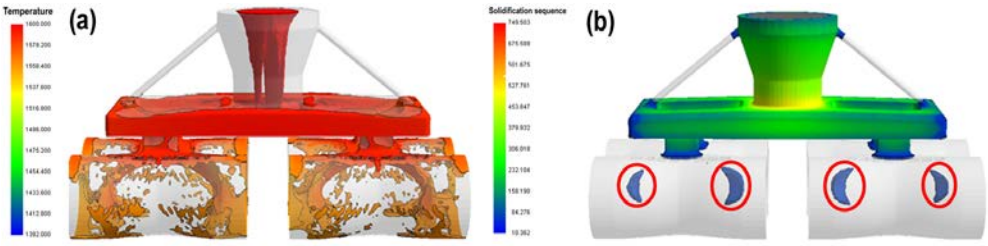


**Fig. 2.** Analysis of filling and solidification processes of liquid metal in initial scheme: (a) filling sequence (t=2.38 s); (b) solidification sequence (t=69.4 s).

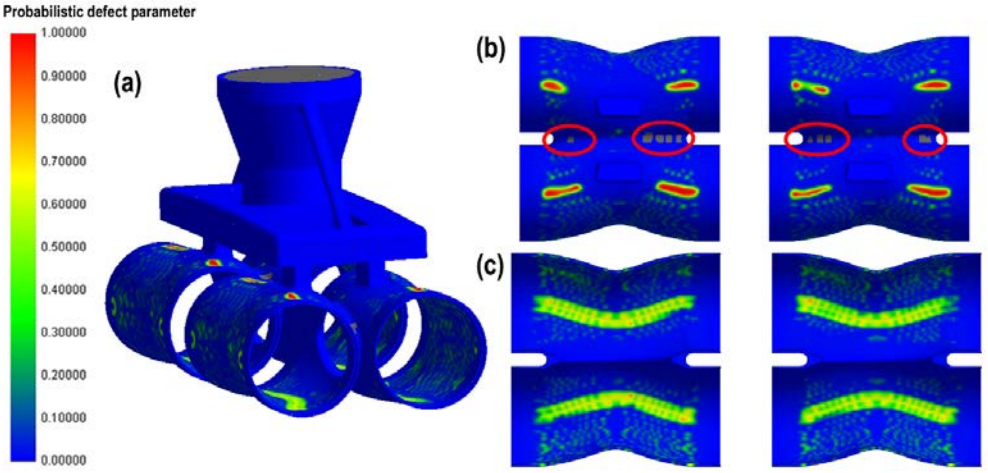


**Fig. 3.** Probabilistic defect distribution of initial scheme: (a) pattern tree; (b) top view of exhaust manifold; (c) bottom view of exhaust manifold.

### 3.2 Design and mold flow analysis of improved scheme for exhaust manifold

Based on the simulation results of the initial scheme, we had the four ingates filled at the same time in the improved scheme and installed two thin boards (L52×W50×H4.5) on both sides of the pipe junctions for solidification feeding. This solved the problems of shrinkage porosity defects, poured short, and turbulent flows. As shown in Fig. 4(a), the liquid metal flowed swiftly toward the thin boards and the bottoms of the exhaust manifold. The splash issue was much improved in the improved scheme, and the flow field of the filling process was much steadier. This prevented air from being captured within cavities and the liquid metal, thereby preventing casting defects caused by the captured air. As shown in Fig. 4(b), the thin boards prompted the feeding of the portions to the left and right of the pipe junctions, and the results show that the isolated residual melt can be effectively concentrated on the board to feed the portions to both sides of the pipe junctions. Figures 5(a) and 5(c) present significantly reduced probabilities of defects at the top and bottom of the exhaust manifold. As shown with the parts circled in red in Fig. 5(b), the installation of the thin boards effectively enabled the filling of the pipe junctions, thereby eliminating the poured short defects in the initial scheme and improving the quality of the casting.

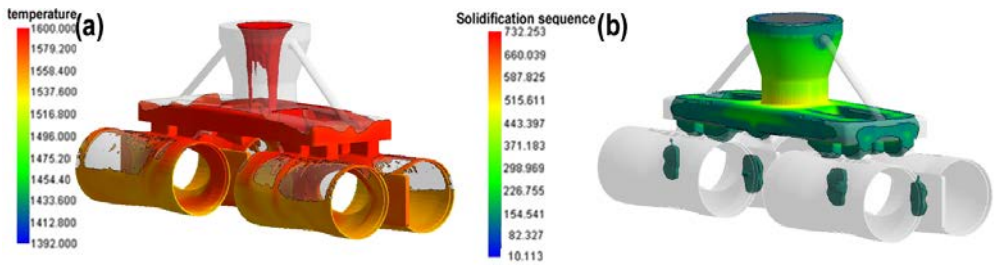


**Fig. 4.** Analysis of filling and solidification processes of liquid metal in improved scheme: (a) filling sequence (t=2.45 s); (b) solidification sequence (t=147.3 s).

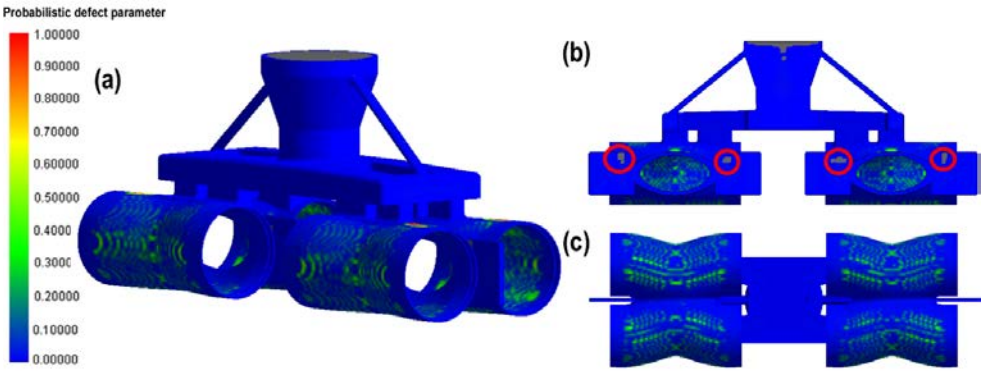


**Fig. 5**. Probabilistic defect distribution of improved scheme: (a) pattern tree; (b) sectional view of exhaust manifold; (c) bottom view of exhaust manifold.

## 4 Conclusions

Increasing the number of ingates and altering their dimensions can effectively improve the stability of the early filling process and reduce turbulent flows. The addition of thin boards at the pipe junctions of the exhaust manifold achieved feeding effects during the solidification process, thereby reducing shrinkage and poured short defects. The simulation results revealed significantly lower probabilities of defects in the improved scheme than in the initial scheme, particularly around the ingates, at the bottom of the exhaust manifold, and at the pipe junctions, which means greater exhaust manifold quality.

## Acknowledgment

The authors gratefully acknowledge the support provided for this research by the Ministry of Science and Technology, R.O.C. under grants MOST 106-2221-E-020 -014 and MOST 106-2622-E-020 -004 -CC3.

## References

1. G.F. Mi, X.Y. Liu, K.F. Wang, J.T. Niu, Numerical simulation of low pressure die-casting aluminum wheel, China Foundry, Vol. 48, No. 1(2009)
2. P.H. Huang, W.J. Wu, C.H. Shieh, Compute-aided design of low die-casting process of A356 aluminum wheels, Applied Mechanics and Materials, Vol. 864, pp. 173-178(2017).
3. P.H. Huang, W.J. Wu, C.H. Shieh, Numerical simulations of low pressure die-casting for A356 aluminum rims, Materials Science Forum, Vol. 893, pp. 276-280(2017).
4. P.H. Huang, Y.T. Chen, B.T. Wang, An effective method for separating casting components from the runner system using vibration-induced fatigue damage, Int J Adv Manuf Technol, Vol. 74, pp. 1275-1282 (2014).
5. P.H. Huang, M.J. Guo, A study on the investment casting of 17-4PH stainless steel helical impeller of centrifugal pump, Materials Research Innovations, 19, S9, 77-81 (2015) DOI 10.1179/1432891715Z.0000000001924
6. P.H. Huang, J.Y. Luo, S.C. Hung, C.J. Lin, H.H. Cheng, Optimal pouring system design for investment casting of cladding thin-plate heater using metallic mold flow Analyses, Applied Mechanics and Materials, Vol. 627, pp. 46-49(2014)

7. P.H. Haung, C.J. Lin, Computer-aided modeling and experimental verification of optimal gating system design for investment casting of precision rotor, Int J Adv Manuf Technol, Vol. 79, pp. 997-1006(2015)
8. J.K. Kuo, P.H. Huang, H.Y. Lai, J.R. Chen, Optimal gating system design for investment casting of 17-4PH stainless steel enclosed impeller by numerical simulation and experimental verification, International Journal of Advanced Manufacturing Technology, 92, 1093-1103 (2017) DOI: 10.1007/s00170-017-0198-0
9. User manual of AnyCasting, version 6.0
10. Y.Y. Li, Prediction of shrinkage defect in steel casting for marine engine cylinder cover by numerical analysis (2007)
11. X.G. Zhao, Z.X. Xiao, J.Z. Guo, Study on the threshold value of simulated shrinkage porosity for a large steel casting, Foundry, Vol. 64, No. 5, pp. 425-429(2015)
12. J.H. Huang, Y. Cao, H.Q. Wang, W.T. Zheng, X.G. Yuan, Casting process design and optimization of martensite stainless steel pumping impeller, Foundry, Vol. 64, No. 4, pp. 317-320(2015).
13. H.B. Ma, H.J. Chuan, Effect of structure of back cover on casting defect and performance, Foundry, Vol. 64, No. 10, pp. 1042-1045(2015)
14. M.Y. Yang, Y.L. Chi, FEM Numerical simulation of temperature and defects prediction algorithm of casting solidification, Foundry, Vol. 66, No. 1, pp. 44-49(2017)
15. S. Li, H.Y. Peng, Solidification process simulation and process optimization for the EPC process of the tail roller, Foundry, Vol. 64, No. 9, pp. 861-863(2015).
16. J. Sun, S.X. Xu, J. Tang, F.F. Wang, Z.Q. Han, Development of squeeze casting technology for manufacturing aluminum alloy subframe for automobile, Foundry, Vol. 64, No. 1, pp. 17-21(2015)
17. S. Li, R.H. Shen, X.G. Yuan, Effect of riser parameters on gray iron feeding, Foundry, Vol. 64, No. 11, pp. 1116-1119(2015)
18. L.W. Pan, L.J. Zheng, H. Zhang, W.L. Gao, Applicability of shrinkage porosity prediction for casting with Niyama criterion, Journal of Beijing University of Aeronautics and Astronautics, Vol. 37, No. 12, pp. 1534-1540(2011)